Nonlinear Dyn (2020) 101:191–209
https://doi.org/10.1007/s11071-020-05753-w

ORIGINAL PAPER

Nonlinear thermal behaviors of the inter-shaft bearing in a dual-rotor system subjected to the dynamic load

Peng Gao · Yushu Chen · Lei Hou

Received: 11 October 2019 / Accepted: 10 June 2020 / Published online: 22 June 2020

Abstract This paper proposes a new theoretical method to investigate the thermal behaviors of the inter-shaft bearing considering the nonlinear dynamic characteristics of a dual-rotor system by combining heat transfer and nonlinear dynamics. The nonlinearities of the inter-shaft bearing, including the Hertzian contact and the radial clearance, are considered during the dynamic modeling for the system. The dynamic load of the inter-shaft bearing is defined according to the nonlinear dynamic responses of the system. Therefore, some fundamental nonlinear phenomena, i.e., jump and bi-stable phenomena happen to the dynamic load. It makes the dynamic load more appropriate to describe the actual load of the inter-shaft bearing than the static load. Furthermore, a steady-state heat transfer model for the inter-shaft bearing subjected to the dynamic load can be set up with the help of Palmgren's empirical formula. The variation of temperatures with the rotation speed is obtained by using the Gauss–Seidel iteration. Temperatures of the inter-shaft bearing also show nonlinear thermal behaviors, i.e., jump and bi-stable phenomena. It implies the nonlinear dynamic behaviors of the system have a great impact on the thermal behaviors of the inter-shaft bearing. Moreover, an exhaustive parametric analysis for temperatures and nonlinear thermal behaviors of the inter-shaft bearing affected by dynamic parameters (including the rotation speed ratio, unbalances of rotors, the radial clearance, the stiffness and the roller number of the inter-shaft bearing) and thermal parameters (including the lubricant viscosity and the ambient temperature) is carried out. The results show that the rotation speed ratio has a significant influence on both temperatures and nonlinear thermal behaviors, other dynamic parameters mainly affect nonlinear thermal behaviors, while thermal parameters only affect temperatures. This unique discovery indicates the thermal behaviors of the inter-shaft bearing could be much more complex because of the nonlinear dynamic characteristics of the dual-rotor system. The obtained results will contribute to a better understanding of the nonlinear thermal behaviors of bearings and profoundly reveal the mechanism of the nonlinear thermal behaviors of bearings.

Keywords Jump phenomenon · Bi-stable phenomenon · Dynamic load · Steady-state heat transfer · Inter-shaft bearing · Dual-rotor

P. Gao · Y. Chen · L. Hou (✉)
School of Astronautics, Harbin Institute of Technology, Harbin 150001, People's Republic of China
e-mail: houlei@hit.edu.cn

P. Gao
e-mail: gaopeng_hit@126.com

List of symbols

M	Total friction torque
M_1	Friction torque due to the load
M_v	Friction torque due to the viscosity

Q	Total FH
Q_l	Load FH
Q_v	Viscosity FH
Q_r	FH distributed to rollers
Q_i	FH distributed to inner race
Q_o	FH distributed to outer race
f_l	A coefficient depends on the type of roller bearing
f_v	A coefficient depends on the type of roller bearing and the type of lubrication
r_{LP}	Inner radius of LP rotor
d	Nominal bore
r_i	Radius of inner race
D_m	Pitch diameter
r_o	Radius of outer race
D	Nominal outside diameter
r_{HP}	Outside radius of HP outer
d_r	Roller diameter
a_r	Roller length
K_b	Stiffness of the inter-shaft bearing
B	Width of the inter-shaft bearing
A	Area
$\sum \rho_i$	Curvature sum of rollers-inner race contact pair
$\sum \rho_o$	Curvature sum of rollers-outer race contact pair
e_1	LP rotor's unbalance
h	Convective heat transfer coefficient
ε_m	Aspect ratio
V	Line speed
k_{steel}	Thermal conductivity of steel
v	Kinematic viscosity of the lubricant
α	Thermal diffusivity
α_{steel}	Thermal diffusivity of steel
A_{down}	"Jump point"
B_{down}	"Jump point"
$\omega_{A_{down}}$	"Frequency of jump point"
$\omega_{B_{down}}$	"Frequency of jump point"
$\Delta T_{A_{down}}$	"Jump amplitude"
$\Delta T_{B_{down}}$	"Jump amplitude"
$\Delta\omega_A$	"Bi-stable interval"
T	Common temperature
T_L	Temperature of lubricant
T_r	Temperature of rollers
T_i	Temperature of inner race
T_o	Temperature of outer race
T_{LP}	Temperature of the portion of LP rotor contact inner race
T_{HP}	Temperature of the portion of HP rotor contact outer race
T_∞	Ambient temperature
R_{ri}	Thermal resistance of rollers-inner race
R_{ro}	Thermal resistance of rollers-outer race
R_{Lr}	Thermal resistance of lubricant rollers
R_{Li}	Thermal resistance of lubricant-inner race
R_{Lo}	Thermal resistance of lubricant-outer race
R_i	Thermal resistance of inner race-LP rotor
R_o	Thermal resistance of outer race-HP rotor
R_{LP}	Thermal resistance of LP rotor-ambient
R_{HP}	Thermal resistance of HP rotor-ambient
F_b	Dynamic load of the inter-shaft bearing
F_n	Normal force between roller and races
$2\delta_0$	Radial clearance of the inter-shaft bearing
N_b	Roller number of the inter-shaft bearing
n_b	Stressed roller number
ω_1	Rotation speed of LP rotor
ω_2	Rotation speed of HP rotor
λ	Rotation speed ratio
e_2	HP rotor's unbalance
Nu	Nusselt number
Re	Reynolds number
Pr	Prandtl number
Ta	Taylor number
Bi	Biot number
Pe	Peclet number
Pe^*	Modified Peclet number
A_{up}	"Jump point"
B_{up}	"Jump point"
$\omega_{A_{up}}$	"Frequency of jump point"
$\omega_{B_{up}}$	"Frequency of jump point"
$\Delta T_{A_{up}}$	"Jump amplitude"
$\Delta T_{B_{up}}$	"Jump amplitude"
$\Delta\omega_B$	"Bi-stable interval"

1 Introduction

With the development of the rotor system trending toward high-speed and heavy-load, higher requirements are put forward for dynamic and thermal performances of the supporting system. Dynamic and thermal behaviors of inter-shaft bearings [1], as essential support and transmission parts between the lower pressure (LP) rotor and the higher pressure (HP) rotor of dual-rotor systems especially in aero engines

of fighters, are much more complex or maybe even nonlinear [2] in many cases. Nevertheless, the research about nonlinear thermal behaviors of the inter-shaft bearing is almost blank at present. Therefore, it is imperative to study nonlinear thermal behaviors of the inter-shaft bearing and clarify the effect of dynamic and thermal parameters.

The effect of bearings' nonlinearities, including the Hertzian contact and the radial clearance on dynamic behaviors of the rotor system, have been discussed by many researchers so far. Yamamoto [3] studied the resonance of a rotor-bearing system affected by the radial clearance of the bearing and discovered that the frequency and amplitude of the resonance peak decrease with the increase of radial clearance. Fukata et al. [4] researched the radial vibration of a ball bearing under a constant radial load and revealed nonlinear vibrations, such as super-harmonic vibration and sub-harmonic vibration, are caused by the Hertzian contact and the radial clearance of bearings. The nonlinear dynamic behaviors, such as jump phenomenon, sub-harmonic and combination vibrations, in an actual dual-rotor assembly for a medium-size jet engine, were reproduced by Holmes [2] on a test facility. Mevel and Guyader [5] described two different routes, i.e., the sub-harmonic route and the quasi-periodic route, to the chaos of a lightly loaded ball bearing based on the same dynamic model of Fukata. A modified harmonic balance method was applied by Tiwari et al. [6, 7] to theoretically simulate the effect of the Hertzian contact and the radial clearance of bearings on nonlinear dynamic behaviors of horizontal rotors and was experimentally verified. Ghafari et al. [8] presented a lumped mass-damper-spring model considering the nonlinear stiffness of rolling elements to investigate the effect of the radial clearance on the equilibrium point of the bearing. Bai et al. [9] established a six degree-of-freedom (6DOF) model to investigate the sub-harmonic resonance of a symmetric ball bearing rotor system by numerical analysis and experiments. Based on the analytic method, also named as HB-AFT applied in Ref. [6, 7], Zhang et al. [10, 11] focused on the resonant hysteresis of a ball bearing rotor system with the Hertzian contact and the radial clearance of bearings. In all of the above works, they all concentrated on the nonlinear dynamic behaviors of bearing rotor system; none of them considered the thermal effect of the bearings.

There indeed exist some excellent research about the thermal behaviors of rolling bearings in the past decades. Palmgren [12] pioneered an empirical formula for calculating the friction torque through numerous experiments on various types and sizes of rolling bearings. Harris [13] utilized the basic concept of heat transfer among the main components of bearings to predict the steady-state temperatures by the lumped parameter method. Winer et al. [14] constructed an apparatus to simulate the thermal behaviors of a tapered roller bearing and offered formulas of thermal resistances between the shaft, the bearing and the housing. A 5DOF model of the rolling bearing was set up by DeMul et al. [15, 16] to describe the relationship between load and deflection by a matrix method. Jorgensen and Shin [17] presented a quasi-three-dimensional heat transfer model to predict the steady-state temperature distribution of the spindle bearing system considering thermal growth. Based on Palmgren's empirical formula, Stein and Tu [18] proposed a state-space model for monitoring the preload of an angular contact ball bearing induced by the thermal expansion and analyzed the effect of the rotation speed and the initial preload. Sun et al. [19] developed an approach for blade loss simulation and established a thermal model to estimate thermal growths of the main components of bearings during the blade loss event. Takabi and Khonsari [20] put forward an unsteady-state heat transfer model for an oil bath lubrication deep-groove ball bearing to study the transient temperatures of the bearing. Ai et al. [21] concentrated on the thermal behaviors of double-row tapered roller bearings lubricated with grease and proposed a quasi-static model for the bearing to attain the load distribution and kinematic parameters. Than and Huang [22] offered a unified method, which is a combination of a quasi-static model and finite element method, to research nonlinear thermal behaviors of a high-speed spindle bearing under preload. Nevertheless, none of the above literatures considers the effect of dynamic characteristics on thermal behaviors of rolling bearings during modeling.

The motivation of this paper is to propose a new theoretical method to investigate the thermal behaviors of the inter-shaft bearing considering the nonlinear dynamic characteristics of a dual-rotor system by combining heat transfer and nonlinear dynamics. The dynamic load of the inter-shaft bearing is defined according to the nonlinear dynamic responses of the

dual-rotor system, which can be substituted into the steady-state heat transfer model of the inter-shaft bearing with the help of Palmgren's empirical formula. Therefore, the model enables us to investigate the thermal behaviors of the inter-shaft bearing affected by the nonlinear dynamic characteristics of the dual-rotor system through numerical simulations. The obtained results show that the nonlinear dynamic load from the dual-rotor system can make significant effect on the thermal behaviors of the inter-shaft bearing, e.g., the temperature frequency curve of the inter-shaft bearing has nonlinear features. In conclusion, the dynamic load defined in this paper is more appropriate than the static load employed in most of the references to describe the actual load of the inter-shaft bearing.

2 Dynamic load of the inter-shaft bearing

CFM56 is one of most widely used dual-rotor aero engines [23]. A two-disk dual-rotor system supported by four points is obtained Based on the basic structure of CFM56 and the simplified method of dynamic model [24]. Figure 1 displays the schematic diagram of a simple dual-rotor system with an inter-shaft bearing [24, 25]. Each rotor is composed of one disk and one shaft, both of which are bound together into one complete rotor. The inter-shaft bearing is located between the LP rotor and the HP rotor. Different from the supporting bearing, both the inner race and the outer race of the inter-shaft bearing rotate with the LP rotor and the HP rotor. Wherein, l_i (i = 1–5) are lengths of shafts, k_i and c_i (i = 1, 2, 3) are stiffness and damping coefficients of springs, ω_1 and ω_2 (rad/s) are rotation speeds of the LP rotor and the HP rotor. Assume that the LP rotor and the HP rotor operate at a constant ratio. Therefore, the rotation speed ratio is defined as $\lambda = \frac{\omega_2}{\omega_1}$. Since the HP rotor rotates faster than the LP rotor, $\lambda > 1$ for the co-rotating system and $\lambda < -1$ for the counter-rotating system.

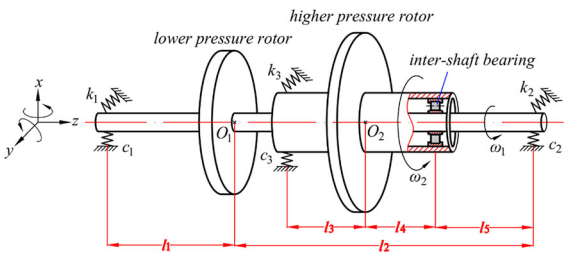

Fig. 1 Schematic diagram of a simple dual-rotor system with an inter-shaft bearing

The mathematical derivation of the dynamic equations for the dual-rotor system has been processed in Ref. [26, 27]. Thus the deduction process is omitted and the dynamic equations are given directly as

$$\begin{aligned} &m_1\ddot{x}_1 + c_1\left(\dot{x}_1 - \dot{\theta}_y l_1\right) + c_2\left(\dot{x}_1 + \dot{\theta}_y l_2\right) \\ &\quad + k_1\left(x_1 - \theta_y l_1\right) + k_2\left(x_1 + \theta_y l_2\right) \\ &\quad = m_1\omega_1^2 e_1\cos(\omega_1 t) - F_x - m_1 g, \end{aligned} \tag{1a}$$

$$\begin{aligned} &m_1\ddot{y}_1 + c_1\left(\dot{y}_1 + \dot{\theta}_x l_1\right) + c_2\left(\dot{y}_1 - \dot{\theta}_x l_2\right) \\ &\quad + k_1\left(y_1 + \theta_x l_1\right) + k_2\left(y_1 - \theta_x l_2\right) \\ &\quad = m_1\omega_1^2 e_1\sin(\omega_1 t) - F_y, \end{aligned} \tag{1b}$$

$$\begin{aligned} &J_{d_1}\ddot{\theta}_x + \omega_1 J_{p_1}\dot{\theta}_y + c_1 l_1\left(\dot{y}_1 + \dot{\theta}_x l_1\right) \\ &\quad - c_2 l_2\left(\dot{y}_1 - \dot{\theta}_x l_2\right) + k_1 l_1\left(y_1 + \theta_x l_1\right) \\ &\quad - k_2 l_2\left(y_1 - \theta_x l_2\right) = F_y(l_2 - l_5), \end{aligned} \tag{1c}$$

$$\begin{aligned} &J_{\mathrm{d}_1}\ddot{\theta}_y - \omega_1 J_{\mathrm{p}_1}\dot{\theta}_x - c_1 l_1\left(\dot{x}_1 - \dot{\theta}_y l_1\right) \\ &\quad + c_2 l_2\left(\dot{x}_1 + \dot{\theta}_y l_2\right) - k_1 l_1\left(x_1 - \theta_y l_1\right) \\ &\quad + k_2 l_2\left(x_1 + \theta_y l_2\right) = -F_x(l_2 - l_5), \end{aligned} \tag{1d}$$

$$\begin{aligned} &m_2\ddot{x}_2 + c_3\left(\dot{x}_2 - \dot{\varphi}_y l_3\right) + k_3\left(x_2 - \varphi_y l_3\right) \\ &\quad = m_2\omega_2^2 e_2\cos(\omega_2 t) + F_x - m_2 g, \end{aligned} \tag{1e}$$

$$\begin{aligned} &m_2\ddot{y}_2 + c_3(\dot{y}_2 + \dot{\varphi}_x l_3) + k_3(y_2 + \varphi_x l_3) \\ &\quad = m_2\omega_2^2 e_2\sin(\omega_2 t) + F_y, \end{aligned} \tag{1f}$$

$$\begin{aligned} &J_{d_2}\ddot{\varphi}_x + \omega_2 J_{p_2}\dot{\varphi}_y + c_3 l_3(\dot{y}_2 + \dot{\varphi}_x l_3) \\ &\quad + k_3 l_3(y_2 + \varphi_x l_3) = -F_y l_4, \end{aligned} \tag{1g}$$

$$\begin{aligned} &J_{\mathrm{d}_2}\ddot{\varphi}_y - \omega_2 J_{\mathrm{p}_2}\dot{\varphi}_x - c_3 l_3\left(\dot{x}_2 - \dot{\varphi}_y l_3\right) \\ &\quad - k_3 l_3\left(x_2 - \varphi_y l_3\right) = F_x l_4, \end{aligned} \tag{1h}$$

The physical significances and values of the parameters in Eq. (1) have been already claimed in Ref. [26, 27].

The inter-shaft bearing is a radial cylindrical roller bearing, especially in the dual-rotor aero engine of the fighter. The nonlinear factors, such as the radial clearance and the fractional exponential relationship

of the Hertzian contact [13], are taken into consideration for calculating restoring forces of the inter-shaft bearing. The schematic diagram of the inter-shaft bearing and the picture of the NU1020 roller bearing are shown in Fig. 2.

The nonlinear vertical and horizontal restoring forces of the inter-shaft bearing [28] are expressed as

$$\begin{bmatrix} F_x \\ F_y \end{bmatrix} = K_{\mathrm{b}} \sum_{k=1}^{N_{\mathrm{b}}} \delta_k^{10/9} H(\delta_k) \begin{bmatrix} \cos\theta_k \\ \sin\theta_k \end{bmatrix}, \tag{2}$$

where K_{b}, N_{b} are the Hertz contact stiffness and the roller number of the inter-shaft bearing, $H(\cdot)$ represents the step function.

Assume that deformations are small enough, then the deformation between kth roller and races δ_k is expressed as

$$\begin{aligned} \delta_k = {} & \left\{ \left[x_1 + \theta_y (l_2 - l_5) \right] - \left(x_2 + \varphi_y l_4 \right) \right\} \cos\theta_k \\ & + \left\{ \left[y_1 - \theta_x (l_2 - l_5) \right] - \left(y_2 - \varphi_x l_4 \right) \right\} \sin\theta_k \\ & - \delta_0 \, (k = 1, 2, \ldots, N_{\mathrm{b}}), \end{aligned}$$

where $2\delta_0$ is the radial clearance of the inter-shaft bearing.

The angular position of the kth roller is $\theta_k = \frac{2\pi}{N_{\mathrm{b}}}(k-1) + \omega_{\mathrm{c}} t \ (k = 1, 2, \ldots, N_{\mathrm{b}})$, where $\omega_{\mathrm{c}} = \frac{\omega_1 r_{\mathrm{i}} + \omega_2 r_{\mathrm{o}}}{r_{\mathrm{i}} + r_{\mathrm{o}}}$ denotes the rotation speed of the cage, r_{i}, r_{o} are the radiuses of inner and outer races.

The NU1020 roller bearing of FAG® is adopted as the inter-shaft bearing in this paper, and its important structural parameters are shown in Table 1.

The dynamic load of the inter-shaft bearing is introduced to estimate the actual load of the inter-shaft bearing when the system is operating at a certain rotation speed. The root-mean-square (RMS) [29] of the vertical and horizontal restoring forces is utilized to define the dynamic load; the formula is

$$\begin{aligned} F_{\mathrm{b}} &= \sqrt{\frac{\int_0^T \left((F_x(t) - \bar{F}_x)^2 + (F_y(t) - \bar{F}_y)^2 \right) \mathrm{d}t}{T}} \\ &= \sqrt{\frac{\sum_{i=1}^{N} \left((F_x(i) - \bar{F}_x)^2 + (F_y(i) - \bar{F}_y)^2 \right)}{N}}, \end{aligned} \tag{3}$$

where T is the period of the restoring forces, N is the number of discrete points in one period, $\bar{F}_x$ and $\bar{F}_y$ are

Table 1 Structural parameters of the NU1020 roller bearing

Parameter	Value
Nominal bore d (mm)	100
Radius of inner race r_{i} (mm)	56.5
Pitch diameter D_{m} (mm)	125
Radius of outer race r_{o} (mm)	68.5
Nominal outside diameter D (mm)	150
Width of bearing B (mm)	24
Diameter of roller d_{r} (mm)	12
Length of roller a_{r} (mm)	14
Roller number N_{b}	24
Radial clearance $2\delta_0$ (μm)	20
Hertzian contact stiffness K_{b} (N/m$^{10/9}$)	10^8

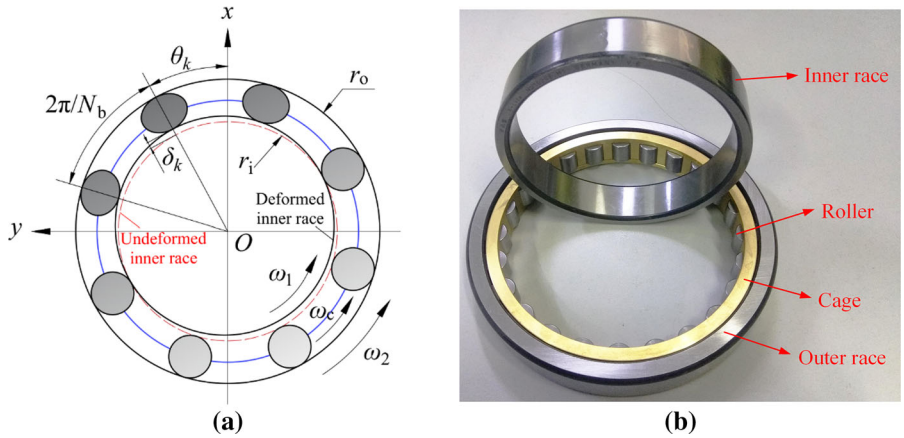

Fig. 2 **a** Schematic diagram of the inter-shaft bearing. **b** The NU1020 roller bearing

average values of vertical and horizontal restoring forces.

3 Heat transfer modeling under the dynamic load

3.1 Friction heat (FH) under the dynamic load

Friction hinders motion and causes energy loss in the form of FH. During the operation of the inter-shaft bearing, FH causes the temperature to rise, which can be measured by the friction torque. The magnitude of friction torque considerably depends on the type of lubrication. For the oil lubrication roller bearing, the lubricant occupies a portion of the free space inside the bearing, and it will hinder the motion of rollers [13]. The friction torque is related to the lubricant performance, the filling amount in the free space, and the rolling speed of rollers.

Nevertheless, these factors are intensely coupled together and extremely difficult to distinguish from each other [18]. In 1959, Palmgren [12] attained an empirical formula for calculating the friction torque through numerous experiments on various types and sizes of rolling bearings. The empirical formula has been widely accepted as a precise method to predict the friction torque.

The inter-shaft bearing is a radial cylindrical roller bearing as shown in Fig. 2, the total friction torque M contains three parts: the load friction torque M_l, and the viscosity friction torque M_v and the roller end-flange friction torque M_f. The inter-shaft bearing do not deliver axial load; thus, M_f can be ignored and M is simplified into

$$M = M_l + M_v, \tag{4a}$$

the unit of above friction torque is N mm.

Different from the static load in previous research [17, 20, 22], the dynamic load of the inter-shaft bearing F_b is introduced to estimate the load friction torque M_l. The dynamic load shows nonlinear behaviors, which makes it much more complex than the static load. The dynamic load is more appropriate to describe the actual load of the inter-shaft bearing than the static load. Therefore, M_l subjected to the dynamic load can be expressed as

$$M_l = f_l F_b D_m, \tag{4b}$$

where f_l is a coefficient depends on the type of roller bearing, its values are shown in Table 2.

The viscosity friction torque M_v is related to the lubricant viscosity apparently. Herein, the kinematic viscosity v in Centistoke (cSt, i.e., mm^2/s) is applied to denote the lubricant viscosity. Both inner and outer races of the inter-shaft bearing rotate with LP and HP rotors; thus, the rotation speed difference between HP and LP rotors $\Delta n = \frac{60}{2\pi}|\omega_2 - \omega_1| = \frac{60}{2\pi}|\lambda - 1|\omega_1$ (r/min, i.e., rpm) is introduced to estimate M_v, as follows:

$$M_v = \begin{cases} 10^{-7} f_v (v \cdot \Delta n)^{2/3} D_m^3 & v \cdot \Delta n \geq 2000 \\ 160 \times 10^{-7} f_v D_m^3 & v \cdot \Delta n < 2000 \end{cases}, \tag{4c}$$

where f_v is a coefficient depends on the type of roller bearing and the type of lubrication, its values are shown in Table 3.

The total FH Q, the load FH Q_l and the viscosity FH Q_v of the inter-shaft bearing are

$$Q = Q_l + Q_v, \tag{5a}$$

$$Q_l = 10^{-3}|\omega_2 - \omega_1|M_l = 10^{-3}|\lambda - 1|\omega_1 M_l, \tag{5b}$$

$$Q_v = 10^{-3}|\omega_2 - \omega_1|M_v = 10^{-3}|\lambda - 1|\omega_1 M_v, \tag{5c}$$

the units of FHs are W.

3.2 Steady-state heat transfer modeling under the dynamic load

The lumped parameter method can be used to set up the steady-state heat transfer model for rollers, inner race and outer race of the inter-shaft bearing, because the Biot number [30] of bearing steel is rather small ($Bi < 0.1$). The inside temperatures of rollers, inner race and outer race are considered the same everywhere, thus the steady-state heat transfer model for the inter-shaft bearing is greatly simplified.

Figure 3 illustrates the thermal network for the inter-shaft bearing. The thermal nodes are labeled in Fig. 3a. There exists six lumped thermal nodes, including T_r, T_i and T_o are rollers, the inner race and the outer race of the inter-shaft bearing; T_{LP} and T_{HP} are portions of LP rotor contact the inner race and HP rotor contact the outer race; T_L is the lubricant. While T_∞ is the temperature of the ambient. The structure sizes of the inter-shaft bearing are also pictured; the values are listed in Table 1. The heat transfer network is depicted in Fig. 3b. R_{ri}, R_{ro}, R_i, R_o are thermal

Table 2 The coefficient f_1 for the cylindrical roller bearing type [13]

Type of cylindrical roller bearing	f_1
Radial cylindrical roller bearing with cage	0.0002–0.0004[a]
Radial cylindrical roller bearing, full complement	0.00055
Thrust cylindrical roller bearing	0.0015

[a]Lower values for light series bearings while higher values for heavy series bearings

Table 3 The coefficient f_v versus cylindrical roller bearing type and lubrication type [13]

Type of cylindrical roller bearing	Type of lubrication			
	Grease	Oil mist	Oil bath	Oil bath (vertical shaft) or oil jet
Cylindrical roller bearing with cage	0.6–1[a]	1.5–2.8[a]	2.2–4[a]	–
Cylindrical roller bearing, full complement	5–10[a]	–	5–10[a]	–
Thrust cylindrical roller bearing	9	–	3.5	8

[a]Lower values for light series bearings while higher values for heavy series bearings

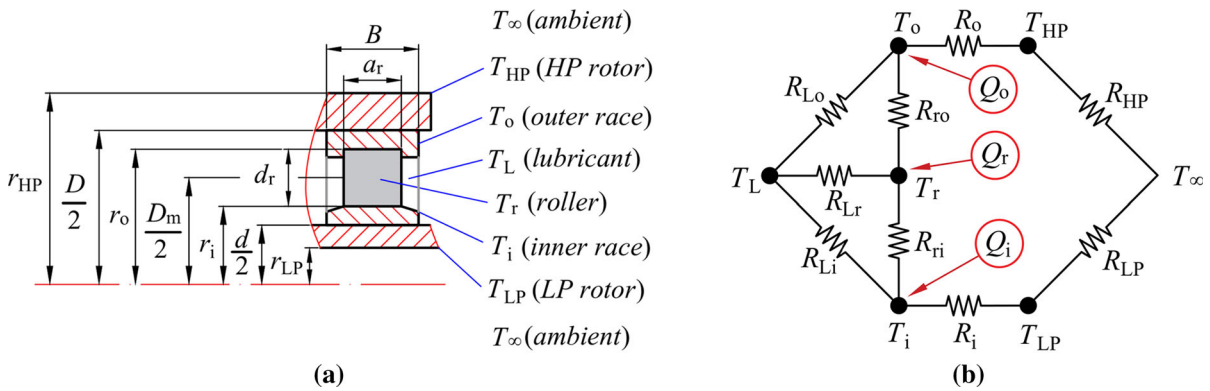

Fig. 3 Thermal network of the inter-shaft bearing. **a** Thermal nodes. **b** Heat transfer network

resistances of heat conduction while R_{Lr}, R_{Li}, R_{Lo}, R_{LP}, R_{HP} are thermal resistances of heat convection.

Assume that FH is generated at the contact zones between rollers and races, then distributed to rollers Q_r, inner race Q_i, and outer race Q_o. The distribution coefficients of the FH refer to Ref. [18]; therefore,

$$Q = Q_r + Q_i + Q_o, \tag{6a}$$

$$Q_r = 0.5Q, \tag{6b}$$

$$Q_i = 0.25Q, \tag{6c}$$

$$Q_o = 0.25Q. \tag{6d}$$

Considering the energy balance for every lumped thermal node, the governing equations of the steady-state heat transfer are expressed as

$$\frac{T_i - T_r}{R_{ri}} + \frac{T_o - T_r}{R_{ro}} + \frac{T_L - T_r}{R_{Lr}} + Q_r = 0, \tag{7a}$$

$$\frac{T_r - T_i}{R_{ri}} + \frac{T_{LP} - T_i}{R_i} + \frac{T_L - T_i}{R_{Li}} + Q_i = 0, \tag{7b}$$

$$\frac{T_r - T_o}{R_{ro}} + \frac{T_{HP} - T_o}{R_o} + \frac{T_L - T_o}{R_{Lo}} + Q_o = 0, \tag{7c}$$

$$\frac{T_{\mathrm{i}}-T_{\mathrm{LP}}}{R_{\mathrm{i}}}+\frac{T_{\infty}-T_{\mathrm{LP}}}{R_{\mathrm{LP}}}=0, \tag{7d}$$

$$\frac{T_{\mathrm{o}}-T_{\mathrm{HP}}}{R_{\mathrm{o}}}+\frac{T_{\infty}-T_{\mathrm{HP}}}{R_{\mathrm{HP}}}=0, \tag{7e}$$

$$\frac{T_{\mathrm{r}}-T_{\mathrm{L}}}{R_{\mathrm{Lr}}}+\frac{T_{i}-T_{\mathrm{L}}}{R_{\mathrm{Li}}}+\frac{T_{\mathrm{o}}-T_{\mathrm{L}}}{R_{\mathrm{Lo}}}=0. \tag{7f}$$

The governing equations of the steady-state heat transfer Eq. (7) can be rewritten in a matrix form as follows:

$$AT=B, \tag{8}$$

where $\boldsymbol{T}=[\,T_{\mathrm{r}}\quad T_{\mathrm{i}}\quad T_{\mathrm{o}}\quad T_{\mathrm{LP}}\quad T_{\mathrm{HP}}\quad T_{\mathrm{L}}\,]^{\mathrm{T}}$, $\boldsymbol{B}=\left[\,-Q_{\mathrm{r}}\quad -Q_{\mathrm{i}}\quad -Q_{\mathrm{o}}\quad -\frac{T_{\infty}}{R_{\mathrm{LP}}}\quad -\frac{T_{\infty}}{R_{\mathrm{HP}}}\quad 0\,\right]^{\mathrm{T}}$, the coefficient matrix $\boldsymbol{A}$ is seen in "Appendix".

3.3 Thermal resistance

(1) Thermal resistance of heat conduction

(a) The thermal resistances of roller-inner race R_{ri} and roller-outer race R_{ro}.

The assumption of ideal line contact is applicable for contact pairs of roller-inner race and roller-outer race, the contact zones are treated as rectangles. The semiwidth of the contact zones [13] can be easily attained as

$$b_i=3.35\times10^{-3}\left(\frac{F_n}{a_r\sum\rho_i}\right)^{\frac{1}{2}},$$
$$b_o=3.35\times10^{-3}\left(\frac{F_n}{a_r\sum\rho_o}\right)^{\frac{1}{2}},$$

where F_{n} is the normal force of roller-race; $\sum\rho_{\mathrm{i}}$ is the curvature sum of roller-inner race contact pair; $\sum\rho_{\mathrm{o}}$ is the curvature sum of roller-outer race contact pair.

The areas of the contact zones of roller-inner race and roller-outer race are

$$A_{\mathrm{i}}=2a_{\mathrm{r}}b_{\mathrm{i}},\quad A_{\mathrm{o}}=2a_{\mathrm{r}}b_{\mathrm{o}}.$$

Considering that the contact zones of roller-inner race and roller-outer race are rectangles, it is not appropriate to use Peclet number [30] directly. The modified Peclet number Pe* [31], which accounts the effect of the shape and orientation of the contact zone, is introduced as follows:

$$\mathrm{Pe}^{*}=(\varepsilon_{\mathrm{m}})^{\frac{1}{2}}\ \mathrm{Pe}=(\varepsilon_{\mathrm{m}})^{\frac{1}{2}}\frac{VL}{\alpha},$$

where $\varepsilon_{\mathrm{m}}=\frac{b}{a}$ is the aspect ratio, which describes the shape and orientation effect of the rectangular or elliptic heat source; V is the line speed; α is the thermal diffusivity; L is the characteristic length depends on the shape of the contact zone, its values are shown in Table 4.

Then the modified Peclet numbers for the contact zones of roller-inner race and roller-outer race are

$$\mathrm{Pe}_{\mathrm{i}}^{*}=(\varepsilon_{\mathrm{m}})^{\frac{1}{2}}\cdot\frac{\omega_1 r_{\mathrm{i}}\sqrt{A_{\mathrm{i}}}}{\alpha_{\mathrm{steel}}},$$
$$\mathrm{Pe}_{\mathrm{o}}^{*}=(\varepsilon_{\mathrm{m}})^{\frac{1}{2}}\cdot\frac{|\lambda\omega_1|r_{\mathrm{o}}\cdot\sqrt{A_{\mathrm{o}}}}{\alpha_{\mathrm{steel}}},$$

where α_{steel} is the thermal diffusivity of steel.

The thermal resistance of one roller-inner race and one roller-outer race [31] are

$$R_{\mathrm{i}}^{\mathrm{one}}=\frac{1.13}{k_{\mathrm{steel}}\sqrt{A_{\mathrm{i}}\cdot\mathrm{Pe}_{\mathrm{i}}^{*}}},$$
$$R_{\mathrm{o}}^{\mathrm{one}}=\frac{1.13}{k_{\mathrm{steel}}\sqrt{A_{\mathrm{o}}\cdot\mathrm{Pe}_{\mathrm{o}}^{*}}}, \tag{9}$$

where k_{steel} is the thermal conductivity of steel.

The stressed roller number of the inter-shaft bearing is represented as n_{b}, i.e., there are n_{b} (a number) $R_{\mathrm{ri}}^{\mathrm{one}}$, $R_{\mathrm{ro}}^{\mathrm{one}}$ in parallel [20]; thus, the total thermal resistances are

$$R_{\mathrm{ri}}=\frac{R_{\mathrm{i}}^{\mathrm{one}}}{n_{\mathrm{b}}},$$
$$R_{\mathrm{ro}}=\frac{R_{\mathrm{o}}^{\mathrm{one}}}{n_{\mathrm{b}}}. \tag{10}$$

(b) The thermal resistances of inner race-LP rotor R_{i} and outer race-HP rotor R_{o}.

Table 4 The characteristic length L for the shape of the contact zone [31]

Shape	Characteristic length
Circular	L= r (r is radius)
Square	L= a (a is length of half side)
Rectangle	L=$\sqrt{A}$ (A is area)
Elliptic	L=$\sqrt{A}$ (A is area)

The inner race-LP rotor and the outer race-HP rotor are interference fit; therefore, the inner race and the portion of LP rotor contact the inner race is treated as singular-layer hollow cylinder; it is the same with the outer race and the portion of HP rotor contact the outer race. Thermal resistances are expressed as

$$R_{\mathrm{i}} = \frac{\ln(d_{\mathrm{i}}/d_{\mathrm{L}})}{2\pi k_{\mathrm{steel}} B}, \quad R_{\mathrm{o}} = \frac{\ln(d_{\mathrm{H}}/d_{\mathrm{o}})}{2\pi k_{\mathrm{steel}} B}. \tag{11}$$

(2) Thermal resistance of heat convection

In order to acquire the thermal resistance of heat convection under different conditions of heat convection [21], it is indispensable to predict the convective heat transfer coefficient h. Nevertheless, h can be expressed in terms of the fluid thermal conductivity k, the characteristic length L and the dimensionless Nusselt number Nu as follows:

$$R_v = \frac{1}{Ah} = \frac{1}{A} \cdot \frac{L}{k \cdot \mathrm{Nu}}. \tag{12}$$

Once the Nusselt number is determined, the thermal resistance of heat convection can be acquired based on Eq. (12). The Nusselt number is measured by the experiment in most cases. The Nusselt numbers under different conditions of heat convection are listed as follows:

(a) The Nusselt number of lubricant roller $\mathrm{Nu_{Lr}}$.

In 1965, Fand [32] presented a correlation by experimental investigation of forced convection from a cylinder to water in crossflow in the range $10^{-1} < \mathrm{Re} < 10^5$. The heat exchange between the lubricant and the cylinder roller meets the requirements of the correlation, which is

$$\mathrm{Nu} = \left(0.35 + 0.34\,\mathrm{Re}^{0.5} + 0.15\,\mathrm{Re}^{0.58}\right) \mathrm{Pr}^{0.3}, \tag{13}$$

the correlation is valid for $10^{-1} < \mathrm{Re} < 10^5$. Where $\mathrm{Re} = \frac{VL}{v}$, $Pr = \frac{v}{\alpha}$ are the dimensionless Reynolds number and the dimensionless Prandtl number.

(b) The Nusselt numbers of lubricant-inner race $\mathrm{Nu_{Li}}$ and lubricant-outer race $\mathrm{Nu_{Lo}}$.

In 1958, Gazley [33] investigated on forced convection between two rotating concentric cylinders, the gap of which is filling with a fluid and air. The inner and outer races are just like two rotating concentric cylinders, which were separated by the lubricant. The Nusselt number is given in Ref. [21] as

$$\mathrm{Nu} = \begin{cases} 2 & \mathrm{Ta} < 41 \\ 0.167\ \mathrm{Ta}^{0.69}\ \mathrm{Pr}^{0.4} & 41 \le \mathrm{Ta} < 100 \\ 0.401\ \mathrm{Ta}^{0.5}\ \mathrm{Pr}^{0.4} & 100 < \mathrm{Ta} \end{cases}, \tag{14}$$

the Taylor number is $Ta = Re\sqrt{\frac{\delta_{\mathrm{io}}}{r}}$, where $\delta_{\mathrm{io}} = \frac{d_{\mathrm{o}} - d_{\mathrm{i}}}{2}$ is the gap between inner and outer races, r is the inside radius of race.

(c) The Nusselt numbers of LP rotor-ambient $\mathrm{Nu_{LP}}$ and HP rotor-ambient $\mathrm{Nu_{HP}}$.

Because LP and HP rotors are rotating, the heat exchange between two rotors and the ambient (air) are forced convection. The Nusselt number is given in Ref. [34] as

$$\mathrm{Nu} = \begin{cases} 0.00308\,\mathrm{Re} + 4.432 & \mathrm{Re} < 7300 \\ \mathrm{Re}^{0.37} & 7300 \le \mathrm{Re} < 9600 \\ 30.5\,\mathrm{Re}^{-0.0042} & 9600 < \mathrm{Re} \end{cases}. \tag{15}$$

4 Results and discussion

4.1 Nonlinear behaviors of the dynamic load

The dynamic equations of the dual-rotor system Eq. (1) are nonlinear due to the nonlinearities of the restoring forces of the inter-shaft bearing. The fourth-order Runge–Kutta method is applied to solve dynamic equations Eq. (1), the dynamic responses are available with the help of the ode45 function in MATLAB®. The RMS is used to express the amplitude in the amplitude frequency curve. Figure 4 displays the amplitude frequency curve of the LP rotor in the dual-rotor system. The dynamic parameters are taken as: the rotation speed ratio $\lambda = 1.2$, the LP rotor's unbalance $e_1 = 3$ μm, the HP rotor's unbalance $e_1 = 2$ μm. The run-up curve represents the rotation speed increases from a lower rotation speed to a higher rotation speed. On the contrary, the run-down curve represents the rotation speed decreases from a higher rotation speed to a lower rotation speed. The amplitude frequency curve of the

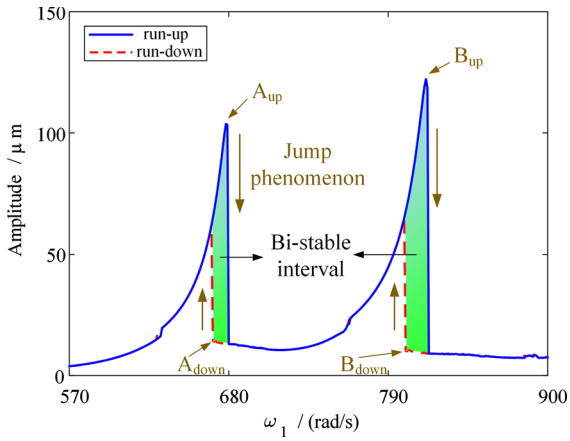

Fig. 4 Amplitude frequency curve of the LP rotor in the dual-rotor system. (Solid lines represent run-up curves, dotted lines represent run-down curves)

HP rotor in the dual-rotor system is omitted because its shape is same with that of the LP rotor.

In Fig. 4, it can be seen that there are two resonance regions, which are caused by double unbalance excitations of HP and LP rotors in both run-up and run-down curves. In the run-up curve, the vibration amplitude increases sharply until the rotation speed reaches $\omega_{A_{up}}$ and $\omega_{B_{up}}$, the jump phenomenon occurs, i.e., the vibration amplitude decrease abruptly; in the run-down curve, the jump phenomenon happens when the rotation speed reduces to $\omega_{A_{down}}$ and $\omega_{B_{down}}$, i.e., the vibration amplitude increases abruptly. When the rotation speed $\omega_1 \in \left[\omega_{A_{down}}, \omega_{A_{up}}\right]$ and $\omega_1 \in \left[\omega_{B_{down}}, \omega_{B_{up}}\right]$, the vibration amplitude in run-up curve do not overlap with that in run-down curve, which means the bi-stable phenomenon occurs. In mathematics, it means Eq. (1) have two stable solutions among two "bi-stable interval" $\left[\omega_{A_{down}}, \omega_{A_{up}}\right]$ and $\left[\omega_{B_{down}}, \omega_{B_{up}}\right]$. Which stable solution the dynamic equations converge to depends on the initial state of motion. The initial states for the run-up curve and the run-down curve at "jump point" A_{down}, A_{up}, B_{down} and B_{up} are different; thus, the run-up curve and the run-down curve do not overlap among "bi-stable interval."

In order to analyze the nonlinear behaviors of dynamic responses in detail, the vibration response analysis for $\omega_1 = 675$ rad/s in the run-up curve and in the run-down curve are shown in Figs. 5 and 6. The analysis methods include the time histories for vertical and horizontal responses, orbit diagrams, Poincaré diagrams, and spectrum diagrams (wherein f_L is the frequency of the LP rotor; f_H is the frequency of the HP rotor; $2f_H - f_L$, $3f_H - 2f_L$ and $f_H + f_L$ are the combination frequencies of the HP rotor with the LP rotor; $2f_H$ is the double frequency of the HP rotor).

Comparing Figs. 5 and 6, the rotation speed are both $\omega_1 = 675$ rad/s; the only difference between them is that Fig. 5 is located in the run-up curve while Fig. 6 is located in the run-down curve. However, the dynamic responses are very different from each other. In Fig. 5, the vertical and horizontal responses are almost harmonic signals, the orbit diagram is circular, the Poincaré diagram only has one point, and f_H is the dominant frequency, f_L is so small that it could be ignored. In Fig. 6, the vertical and horizontal responses are quasi-periodic signals, and look like beat vibrations. The orbit diagram is unclosed circle ring. The Poincaré diagram have six points. f_L and f_H are the dominant frequency, but the combination frequencies ($2f_H - f_L$, $3f_H - 2f_L$ and $f_H + f_L$) and the double frequency ($2f_H$) also occurs.

The restoring forces of the inter-shaft bearing can be attained by substituting the dynamic responses into Eq. (2). The restoring forces of the inter-shaft bearing for $\omega_1 = 675$ rad/s in the run-up curve and in the run-down curve are displayed in Figs. 7 and 8. It can be found the force state of the inter-shaft bearing are very different from each other. The force of Fig. 7 is significantly greater than Fig. 8. Moreover, the restoring forces all vary periodically. The vertical and horizontal restoring forces are variable forces at a certain rotation speed. It is very difficult and inconvenient to describe the actual load of the inter-shaft bearing by using the vertical and horizontal restoring forces.

The dynamic load of the inter-shaft bearing can be obtained by substituting the restoring forces into the definition of the dynamic load Eq. (3). Figure 9 illustrates the variation of the dynamic load versus the rotation speed. It can be found that jump phenomenon also occurs at four "jump point" A_{down}, A_{up}, B_{down} and B_{up}, and bi-stable phenomenon occurs among two "bi-stable interval" $\left[\omega_{A_{down}}, \omega_{A_{up}}\right]$ and $\left[\omega_{B_{down}}, \omega_{B_{up}}\right]$. The dynamic load shows the same behaviors as the vibration amplitude. Comparing with restoring forces, the dynamic load is a constant force at a certain rotation speed. Thus, it is easier and more

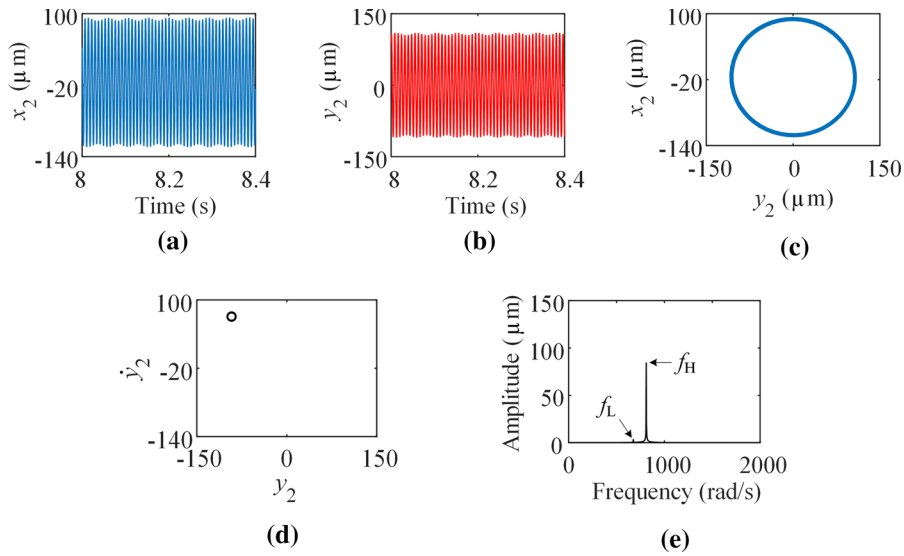

Fig. 5 Vibration response analysis for ω_1 = 675 rad/s in the run-up curve. **a** Vertical response. **b** Horizontal response. **c** Orbit diagram. **d** Poincaré diagram. **e** Spectrum diagram

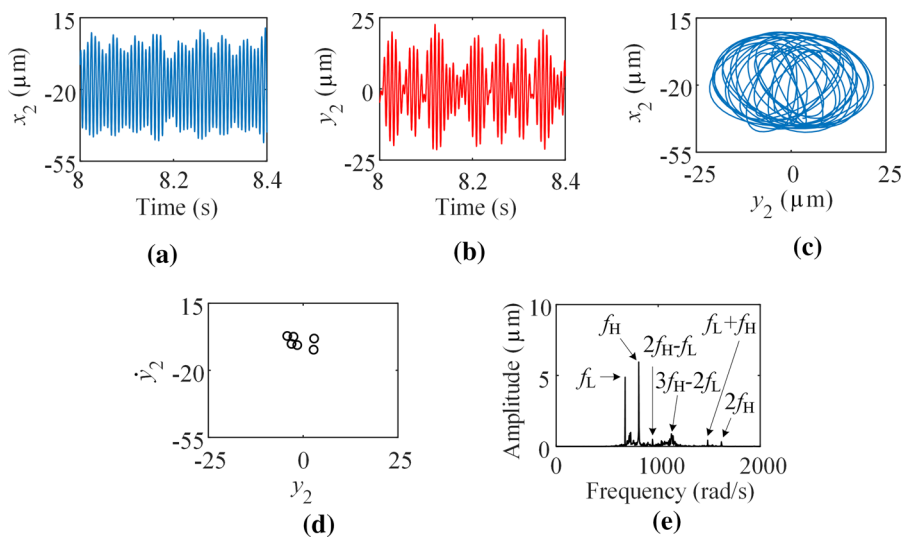

Fig. 6 Vibration response analysis for ω_1 = 675 rad/s in the run-down curve. **a** Vertical response. **b** Horizontal response. **c** Orbit diagram. **d** Poincaré diagram. **e** Spectrum diagram

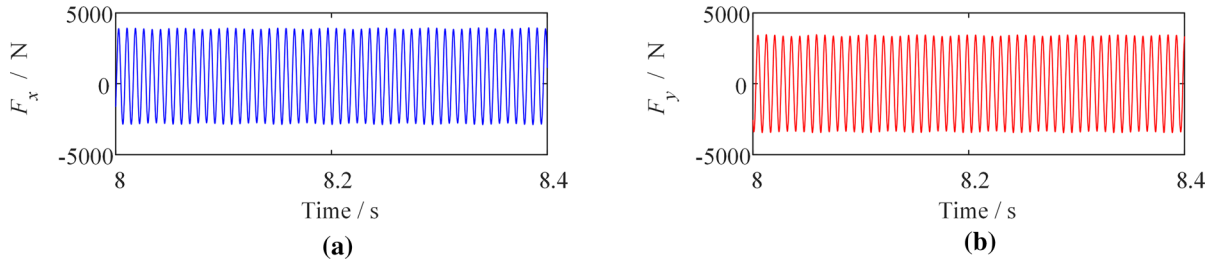

Fig. 7 The restoring forces of the inter-shaft bearing for ω_1 = 675 rad/s in the run-up curve. **a** Vertical restoring force. **b** Horizontal restoring force

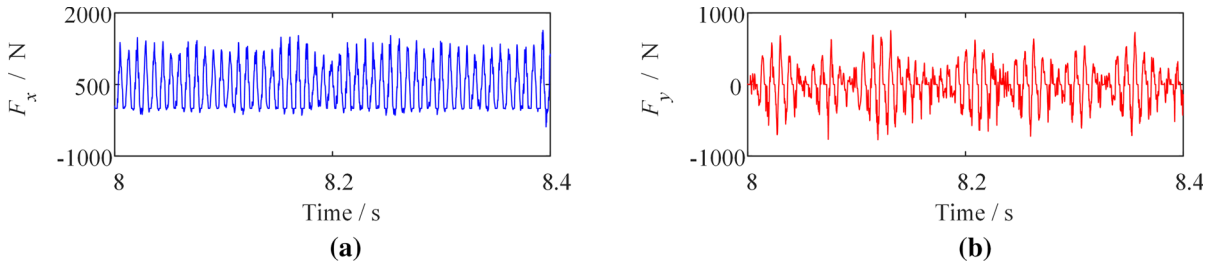

Fig. 8 The restoring forces of the inter-shaft bearing for $\omega_1 = 675$ rad/s in the run-down curve. **a** Vertical restoring force. **b** Horizontal restoring force

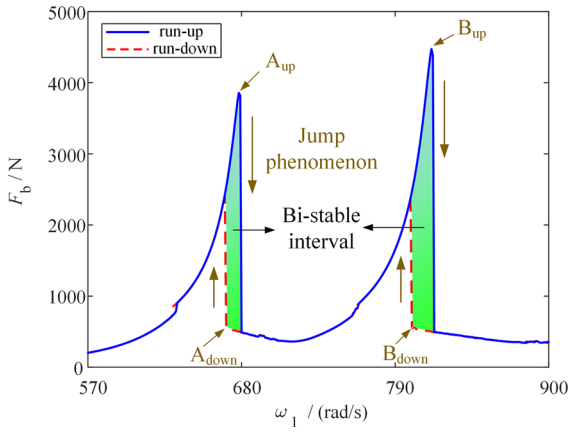

Fig. 9 Variation of dynamic load with rotation speed. (Solid lines represent run-up curves, dotted lines represent run-down curves)

convenient to describe the actual load of the inter-shaft bearing.

In a word, the nonlinearities of the inter-shaft bearing, including the radial clearance and the fractional exponential relationship of the Hertzian contact, are considered during the dynamic modeling for the dual-rotor system. The dynamic load of the inter-shaft bearing is defined according to the nonlinear dynamic responses of the system. The dynamic load shows nonlinear behaviors, i.e., jump and bi-stable phenomena. It means the dynamic load can reflect the nonlinear dynamic characteristics of the system, which makes it much more complex than the static load. In conclusion, the dynamic load defined in this paper is more appropriate than the static load employed in most of the references to describe the actual load of the inter-shaft bearing.

4.2 Nonlinear thermal behaviors

The governing equations of steady-state heat transfer for the inter-shaft bearing Eq. (8) are linear matrix equations. The Gauss–Seidel iteration, an indirect method, is applied to solve the linear matrix equations, because the coefficient matrix $\boldsymbol{A}$ may be an ill condition [35] in many cases. The error of the Gauss–Seidel iteration for every rotation speed is set as $\left\|\boldsymbol{T}^{(n)} - \boldsymbol{T}^{(n-1)}\right\| \leq 10^{-12}$ (n denotes iteration time). The variation for temperatures of rollers, inner race and outer race with rotation speed, is plotted in Fig. 10. Thermal parameters are taken as: the lubricant viscosity $v = 5$ mm^2/s, the ambient temperature $T_\infty = 20$ °C.

In Fig. 10, it can be observed that the temperature of rollers T_r higher than the temperature of inner race T_i higher than the temperature of outer race T_o in both run-up and run-down curves, i.e., $T_\mathrm{r} > T_\mathrm{i} > T_\mathrm{o}$. Nevertheless, the variation of T_r, T_i and T_o in both run-up

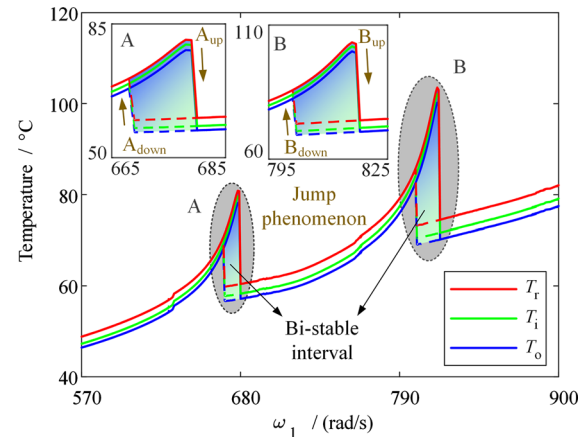

Fig. 10 Variation for temperatures of rollers, inner race and outer race with rotation speed. (Solid lines represent run-up curves, dotted lines represent run-down curves)

and run-down curves with rotation speed are the same with each other. Therefore, we take T_r as an example to analyze nonlinear thermal behaviors of the inter-shaft bearing in the following sections. In the resonance regions A and B, T_r in run-up curve rises sharply until the rotation speed reaches $\omega_{A_{up}}$ and $\omega_{B_{up}}$, the jump phenomenon happens, i.e., T_r declines abruptly; T_r in run-down curve declines gradually until the rotation speed reduces to $\omega_{A_{down}}$ and $\omega_{B_{down}}$, the jump phenomenon happens, i.e., T_r rises abruptly. When the rotation speed $\omega_1 \in \left[\omega_{A_{down}}, \omega_{A_{up}}\right]$ and $\omega_1 \in \left[\omega_{B_{down}}, \omega_{B_{up}}\right]$, T_r in run-up curve do not overlap with T_r in run-down curve, which implies the bi-stable phenomenon happens.

In order to further analyze nonlinear thermal behaviors in the following sections, we introduce some symbols and parameters as: A_{down}, A_{up}, B_{down} and B_{up} are named as "jump point"; $\omega_{A_{down}}$, $\omega_{A_{up}}$, $\omega_{B_{down}}$ and $\omega_{B_{up}}$ are named as "frequency of jump point"; $\Delta T_{A_{down}}$, $\Delta T_{A_{up}}$, $\Delta T_{B_{down}}$ and $\Delta T_{B_{up}}$ are named as "jump amplitude"; $\Delta\omega_A = \left[\omega_{A_{down}}, \omega_{A_{up}}\right]$ and $\Delta\omega_B = \left[\omega_{B_{down}}, \omega_{B_{up}}\right]$ are named as "bi-stable interval."

It is vital to carry out the FH analysis, including the total FH, the load FH and the viscosity FH, for exploring the inherent mechanism of nonlinear thermal behaviors of the inter-shaft bearing. Figure 11 displays the variation of the total FH, the load FH and the viscosity FH with rotation speed. The solid lines denote run-up curves and the dotted lines denote run-down curves.

In Fig. 11, the blue line represents the viscosity FH Q_v, Q_v increases gradually with the increase of rotation speed, no nonlinear thermal behavior happens. The green line represents the load FH Q_l, Q_l shows jump phenomenon at "jump point" A_{up} and B_{up} in run-up curve while at "jump point" A_{down} and B_{down} in run-down curve; bi-stable phenomenon happens among two "bi-stable interval" $\Delta\omega_A$ and $\Delta\omega_B$. The red line represents the total FH Q, Q increases gradually with the increase of the rotation speed beyond $\Delta\omega_A$ and $\Delta\omega_B$; Q shows jump phenomenon at A_{up} and B_{up} in run-up curve while at A_{down} and B_{down} in run-down curve; bi-stable phenomenon happens among $\Delta\omega_A$ and $\Delta\omega_B$.

In a word, the direct reason why temperatures of the inter-shaft bearing show nonlinear thermal behaviors, i.e., jump and bi-stable phenomena, is the load FH shows nonlinear behaviors, while the root reason is the nonlinear dynamic characteristics of the dual-rotor system. The dynamic load of the inter-shaft bearing is introduced to calculate the load FH. The dynamic load can reflect the nonlinear dynamic characteristics of the dual-rotor system. This unique discovery cannot be found if the static load is applied to calculate the load FH.

4.3 Effect of rotation speed ratio

The effect of the rotation speed ratio on temperatures and nonlinear thermal behaviors of the inter-shaft bearing is discussed in this section, the rotation speed

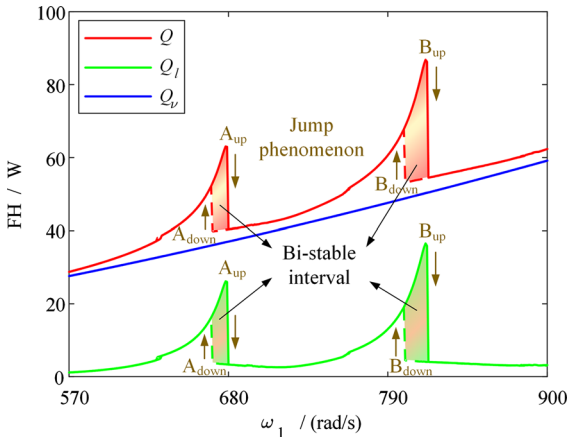

Fig. 11 Variation of the total FH, the load FH and the viscosity FH with rotation speed. (Solid lines represent run-up curves, dotted lines represent run-down curves)

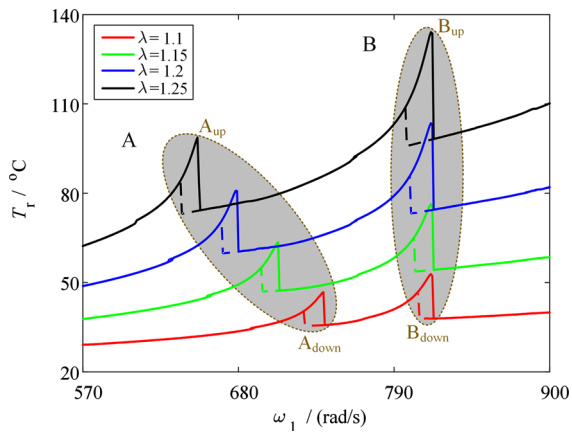

Fig. 12 Variation for temperature of rollers with rotation speed under different rotation speed ratio. (Solid lines represent run-up curves, dotted lines represent run-down curves)

ratio are $\lambda = 1.1$, $\lambda = 1.15$, $\lambda = 1.2$ and $\lambda = 1.25$. The variation for temperature of rollers with rotation speed under different rotation speed ratio are depicted in Fig. 12.

In Fig. 12, with the increase of rotation speed ratio λ, the temperature of rollers T_r rises obviously; "frequency of jump point" $\omega_{B_{down}}$ and $\omega_{B_{up}}$ are still, but $\omega_{A_{down}}$ and $\omega_{A_{up}}$ decrease obviously; "jump amplitude" $\Delta T_{A_{down}}$, $\Delta T_{A_{up}}$, $\Delta T_{B_{down}}$ and $\Delta T_{B_{up}}$ all increase apparently; "bi-stable interval" $\Delta\omega_A$ and $\Delta\omega_B$ remain the original length, while $\Delta\omega_B$ is wider than $\Delta\omega_A$.

Comparing the values of $\omega_{A_{down}}$, $\omega_{A_{up}}$, $\omega_{B_{down}}$, $\omega_{B_{up}}$ with λ, the approximate relation is as follows:

$$\frac{\omega_{B_{down}}}{\omega_{A_{down}}} \approx \lambda \approx \frac{\omega_{B_{up}}}{\omega_{A_{up}}}. \tag{16}$$

From Eq. (16), it can be seen that the rotation speed ratio has a crucial influence on $\omega_{A_{down}}$ and $\omega_{A_{up}}$. In other words, the rotation speed ratio determines the relative position of four "jump point" and two "bi-stable interval" where nonlinear thermal behaviors happen.

4.4 Effect of rotors' unbalances

The effect of the LP and HP rotors' unbalances on temperatures and nonlinear thermal behaviors of the inter-shaft bearing is discussed in this section. Firstly, the LP rotor's unbalance are $e_1 = 2\mu m$, $e_1 = 3\mu m$, $e_1 = 4\mu m$ and $e_1 = 5\mu m$. The variation for temperature of rollers with rotation speed under different unbalances of LP rotor is depicted in Fig. 13.

In Fig. 13, the temperature of rollers T_r under different LP rotor's unbalances e_1 almost overlap except the resonance region B, which indicates e_1 mostly affects the region B. With the increase of e_1, "frequency of jump point" $\omega_{A_{down}}$ and $\omega_{A_{up}}$ are still, but $\omega_{B_{down}}$ and $\omega_{B_{up}}$ increase sharply; "jump amplitude" $\Delta T_{A_{down}}$ and $\Delta T_{A_{up}}$ barely change, while $\Delta T_{B_{down}}$ and $\Delta T_{B_{up}}$ increase apparently; "bi-stable interval" $\Delta\omega_A$ remains the original length, but $\Delta\omega_B$ becomes narrower.

Finally, the HP rotor's unbalance are $e_2 = 2\mu m$, $e_2 = 3\mu m$, $e_2 = 4\mu m$ and $e_2 = 5\mu m$. The variation for temperature of rollers with rotation speed under different unbalances of HP rotor is depicted in Fig. 14.

In Fig. 14, the temperature of rollers T_r under different HP rotor's unbalances e_2 almost overlap except the resonance region A, which indicates e_2 mostly affects the region A. With the increase of e_2, "frequency of jump point" $\omega_{B_{down}}$ and $\omega_{B_{up}}$ are still, but $\omega_{A_{down}}$ and $\omega_{A_{up}}$ increase sharply; "jump amplitude" $\Delta T_{B_{down}}$ and $\Delta T_{B_{up}}$ barely change, while $\Delta T_{A_{down}}$ and $\Delta T_{A_{up}}$ increase apparently; "bi-stable interval" $\Delta\omega_B$ remains the original length, but $\Delta\omega_A$ becomes narrower.

In summary, the unbalance of LP rotor only affects the resonance region B, while the unbalance of HP rotor only affects the resonance region A. With the increase of corresponding unbalance, the corresponding "frequency of jump point" and "jump amplitude"

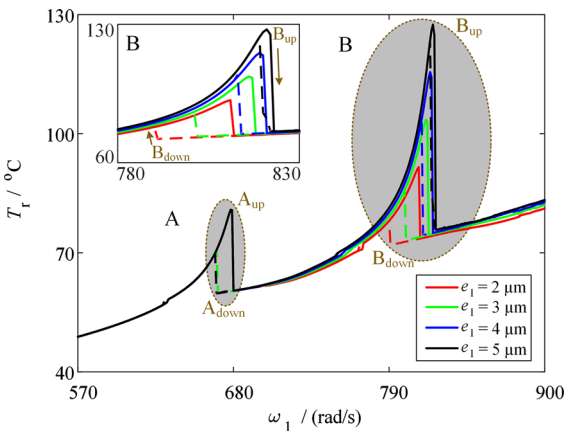

Fig. 13 Variation for temperature of rollers with rotation speed under different unbalances of LP rotor. (Solid lines represent run-up curves, dotted lines represent run-down curves)

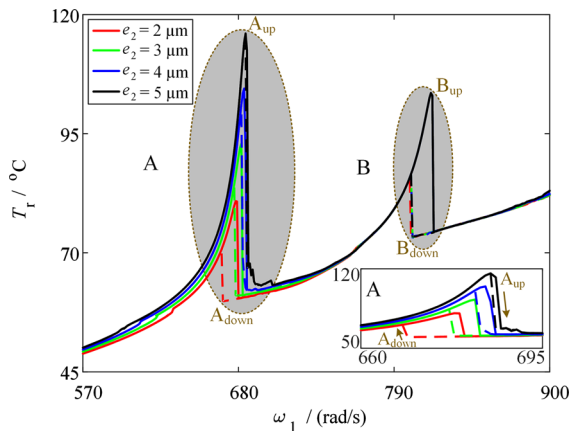

Fig. 14 Variation for temperature of rollers with rotation speed under different unbalances of HP rotor. (Solid lines represent run-up curves, dotted lines represent run-down curves)

increase while the corresponding "bi-stable interval" becomes narrower.

4.5 Effect of inter-shaft bearings' radial clearance

The effect of the inter-shaft bearings' radial clearance on temperatures and nonlinear thermal behaviors of the inter-shaft bearing is discussed in this section, the radial clearance are $\delta_0 = 3\mu m$, $\delta_0 = 5\mu m$, $\delta_0 = 8\mu m$ and $\delta_0 = 10\mu m$. The variation for temperature of rollers with rotation speed under different radial clearance are depicted in Fig. 15.

In Fig. 15, it can be seen that the radial clearance δ_0 has a significant influence on nonlinear thermal behaviors of the inter-shaft bearing. With the increase of δ_0, the highest temperature of T_r barely changes; "frequency of jump point" $\omega_{A_{up}}$ and $\omega_{B_{up}}$ decrease slightly, while $\omega_{A_{down}}$ and $\omega_{B_{down}}$ decrease obviously; "jump amplitude" $\Delta T_{A_{up}}$ and $\Delta T_{B_{up}}$ increase slightly, but $\Delta T_{A_{down}}$ and $\Delta T_{B_{down}}$ increase apparently; "bi-stable interval" $\Delta\omega_A$ and $\Delta\omega_B$ become wider rapidly. It is worth noting that jump and bi-stable phenomena disappear when $\delta_0 = 3\mu m$.

In other words, the radial clearance of the inter-shaft bearing delays the contact between rollers and races, which is equivalent to reducing the stiffness of the inter-shaft bearing in another way [36]; thus, "frequency of jump point" decrease. Moreover, the radial clearance is an essential nonlinearity, thus reducing the radial clearance appropriately will significantly suppress nonlinear thermal behaviors, i.e., reduce "jump amplitude" and narrow "bi-stable interval."

4.6 Effect of inter-shaft bearing's stiffness

The effect of the inter-shaft bearings' stiffness on temperatures and nonlinear thermal behaviors of the inter-shaft bearing is discussed in this section; the stiffness are $K_b = 8K_{b0}$, $K_b = 10K_{b0}$, $K_b = 15K_{b0}$ and $K_b = 20K_{b0}$ ($K_{b0} = 10^7 N/m^{10/9}$). The variation for temperature of rollers with rotation speed under different stiffness are depicted in Fig. 16.

In Fig. 16, it can be seen that the stiffness K_b mostly affects nonlinear thermal behaviors of the inter-shaft bearing. With the increase of K_b, the highest temperature of T_r barely changes; "frequency of jump point" $\omega_{A_{down}}$, $\omega_{A_{up}}$, $\omega_{B_{down}}$ and $\omega_{B_{up}}$ all increase obviously; "jump amplitude" $\Delta T_{A_{down}}$, $\Delta T_{A_{up}}$, $\Delta T_{B_{down}}$ and $\Delta T_{B_{up}}$ decrease slightly; "bi-stable interval" $\Delta\omega_A$ and $\Delta\omega_B$ become narrower slowly.

4.7 Effect of inter-shaft bearing's roller number

The effect of the inter-shaft bearings' roller number on temperatures and nonlinear thermal behaviors of the inter-shaft bearing is discussed in this section; the roller number are $N_b = 12$, $N_b = 16$, $N_b = 20$ and $N_b = 24$. The variation for temperature of rollers with

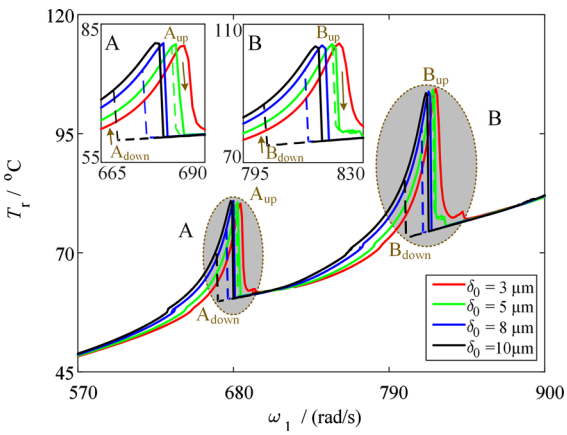

Fig. 15 Variation for temperature of rollers with rotation speed under different radial clearance. (Solid lines represent run-up curves, dotted lines represent run-down curves)

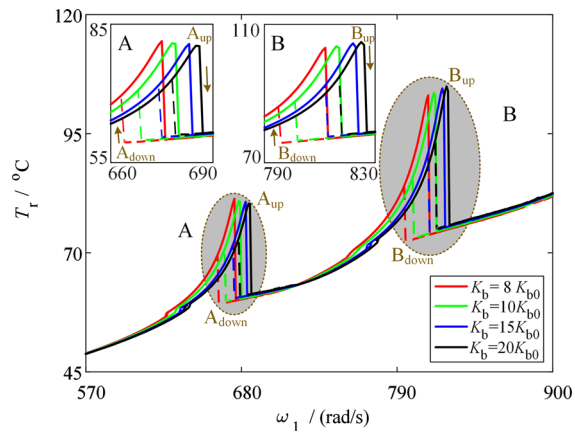

Fig. 16 Variation for temperature of rollers with rotation speed under different stiffness. (Solid lines represent run-up curves, dotted lines represent run-down curves)

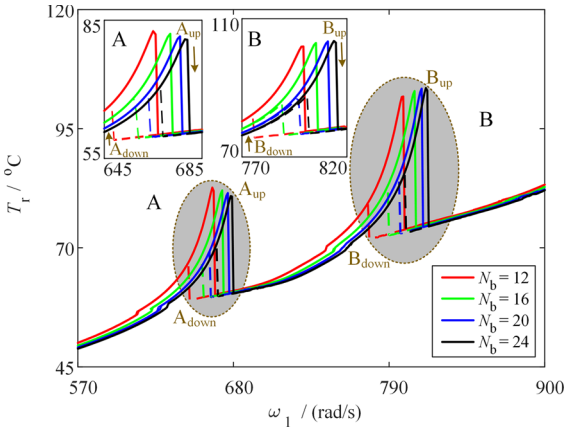

Fig. 17 Variation for temperature of rollers with rotation speed under different roller numbers. (Solid lines represent run-up curves, dotted lines represent run-down curves)

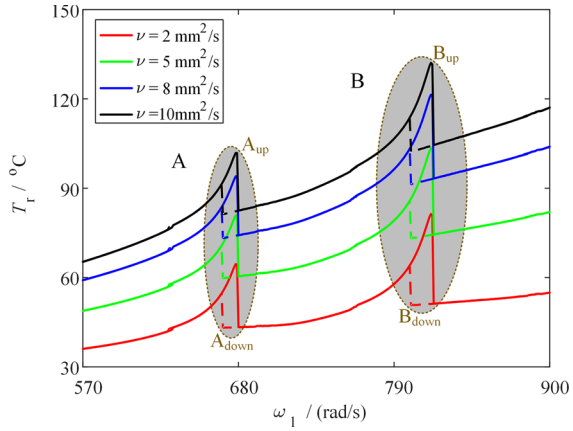

Fig. 18 Variation for temperature of rollers with rotation speed under different lubricant viscosity. (Solid lines represent run-up curves, dotted lines represent run-down curves)

rotation speed under different roller numbers are depicted in Fig. 17.

In Fig. 17, it can be seen that the roller number N_b mostly affects nonlinear thermal behaviors of the inter-shaft bearing. With the increase of N_b, the highest temperature of T_r barely changes; "frequency of jump point" $\omega_{A_{down}}$, $\omega_{A_{up}}$, $\omega_{B_{down}}$ and $\omega_{B_{up}}$ all increase obviously; "jump amplitude" $\Delta T_{A_{down}}$, $\Delta T_{A_{up}}$, $\Delta T_{B_{down}}$ and $\Delta T_{B_{up}}$ decrease slightly; "bi-stable interval" $\Delta\omega_A$ and $\Delta\omega_B$ become narrower slowly.

It is worth noting that the effect of the roller number on nonlinear thermal behaviors is very similar with the stiffness of the inter-shaft bearing. More roller number, more stressed roller number, greater dynamic load, and greater stiffness. Therefore, raising the stiffness and the roller number of the inter-shaft bearing moderately is helpful to suppress nonlinear thermal behaviors, i.e., reduce "jump amplitude" and narrow "bi-stable interval."

4.8 Effect of the lubricant viscosity

The effect of the lubricant viscosity on temperatures and nonlinear thermal behaviors of the inter-shaft bearing is discussed in this section; the lubricant viscosity are $\nu = 2$ mm^2/s, $\nu = 5$ mm^2/s, $\nu = 8$ mm^2/s and $\nu = 10$ mm^2/s. The variation for temperature of rollers with rotation speed under different lubricant viscosity are depicted in Fig. 18.

In Fig. 18, it can be seen that the lubricant viscosity ν has a significant influence on temperatures of the inter-shaft bearing. With the increase of ν, the temperature of rollers T_r rises sharply; "frequency of jump point" $\omega_{A_{down}}$, $\omega_{A_{up}}$, $\omega_{B_{down}}$ and $\omega_{B_{up}}$ are still; "jump amplitude" $\Delta T_{A_{down}}$, $\Delta T_{A_{up}}$, $\Delta T_{B_{down}}$ and $\Delta T_{B_{up}}$ barely change; "bi-stable interval" $\Delta\omega_A$ and $\Delta\omega_B$ remains the original length.

4.9 Effect of the ambient temperature

The effect of the ambient temperature on temperatures and nonlinear thermal behaviors of the inter-shaft bearing is discussed in this section; the ambient temperature are $T_\infty = 20$ °C, $T_\infty = 30$ °C, $T_\infty = 40$ °C and $T_\infty = 50$ °C. The variation for temperature

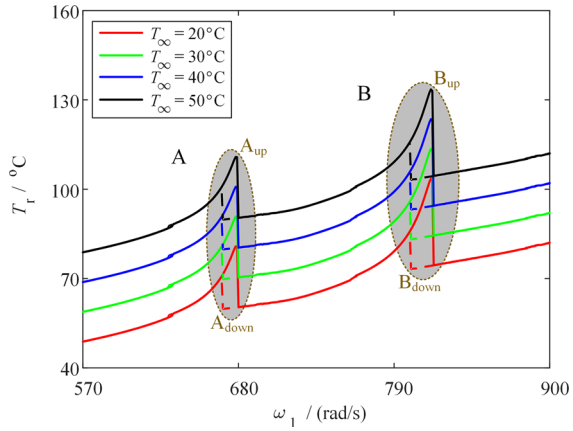

Fig. 19 Variation for temperature of rollers with rotation speed under different ambient temperatures. (Solid lines represent run-up curves, dotted lines represent run-down curves)

of rollers with rotation speed under different ambient temperatures is depicted in Fig. 19.

In Fig. 19, it can be seen that the ambient temperature T_∞ has a significant influence on temperatures of the inter-shaft bearing. With the increase of T_∞, the temperature of rollers T_r rises sharply; "frequency of jump point" $\omega_{A_{down}}$, $\omega_{A_{up}}$, $\omega_{B_{down}}$ and $\omega_{B_{up}}$ are almost still; "jump amplitude" $\Delta T_{A_{down}}$, $\Delta T_{A_{up}}$, $\Delta T_{B_{down}}$ and $\Delta T_{B_{up}}$ barely change; "bi-stable interval" $\Delta\omega_A$ and $\Delta\omega_B$ remains the original length.

It is worthwhile to note that the effect of the lubricant viscosity and the ambient temperature is the same with each other. They both have a significant influence on temperatures of the inter-shaft bearing, while no effect on nonlinear thermal behaviors. Therefore, reducing the lubricant viscosity and the ambient temperature appropriately is contributive to control temperatures of the inter-shaft bearing.

5 Conclusions

In this paper, the dynamic load of the inter-shaft bearing has been defined according to the nonlinear dynamic responses of a dual-rotor system, based on which, a steady-state heat transfer model for the inter-shaft bearing subjected to the dynamic load has been set up with the help of Palmgren's empirical formula. Thermal behaviors of the inter-shaft bearing affected by the nonlinear dynamic characteristics of the system have been studied in detail. Furthermore, an exhaustive parametric analysis for temperatures and nonlinear thermal behaviors of the inter-shaft bearing affected by dynamic and thermal parameters has been carried out. Some meaningful conclusions are drawn as follows:

(1) The dynamic load can reflect the nonlinear dynamic characteristics of the dual-rotor system. It is more appropriate than the static load employed in most of the references to describe the actual load of the inter-shaft bearing.

(2) Nonlinear thermal behaviors, i.e., jump and bi-stable phenomena, happen to temperatures of the inter-shaft bearing. There exists two "jump point" in both the run-up curve and the run-down curve, and two "bi-stable interval" are formed between the corresponding "jump point."

(3) The rotation speed ratio has a significant influence on both temperatures and nonlinear thermal behaviors of the inter-shaft bearing. Reducing the rotation speed ratio reasonably is not only helpful to curb temperatures, but also helpful to suppress nonlinear thermal behaviors.

(4) Dynamic parameters mainly affect nonlinear thermal behaviors of the inter-shaft bearing. Reducing unbalances of rotors and the radial clearance or raising the stiffness and the roller number moderately are conducive to reduce "jump amplitude" and narrow "bi-stable interval."

(5) Thermal parameters only affect temperatures of the inter-shaft bearing. Reducing the lubricant viscosity and the ambient temperature appropriately are contributive to control temperatures at a lower level.

The unique discovery in this paper indicates the thermal behaviors of the inter-shaft bearing could be much more complex due to the nonlinear dynamic characteristics of the dual-rotor system. The future work will concentrate on the experimental verification of nonlinear thermal behaviors.

Acknowledgements The authors are very grateful for the financial supports from the National Major Science and Technology Projects of China (Grant No. 2017-IV-0008-0045), the National Basic Research Program of China (973 Program) (Grant No. 2015CB057400) and the National Natural Science Foundation of China (Grant Nos. 11972129 and 11602070).

Compliance with ethical standards

Conflict of interest The authors declare that they have no conflict of interest.

Appendix

The coefficient matrix $\boldsymbol{A}$ is a symmetric matrix, which is shown as follows:

$$A = \begin{bmatrix} -\frac{1}{R_{ri}} - \frac{1}{R_{ro}} - \frac{1}{R_{Lr}} & \frac{1}{R_{ri}} & \frac{1}{R_{ro}} & & & \frac{1}{R_{Lr}} \\ \frac{1}{R_{ri}} & -\frac{1}{R_{ri}} - \frac{1}{R_i} - \frac{1}{R_{Li}} & & \frac{1}{R_i} & & \frac{1}{R_{Li}} \\ \frac{1}{R_{ro}} & & -\frac{1}{R_{ro}} - \frac{1}{R_o} - \frac{1}{R_{Lo}} & & \frac{1}{R_o} & \frac{1}{R_{Lo}} \\ & \frac{1}{R_i} & & -\frac{1}{R_i} - \frac{1}{R_{LP}} & & \\ & & \frac{1}{R_o} & & -\frac{1}{R_o} - \frac{1}{R_{HP}} & \\ \frac{1}{R_{Lr}} & \frac{1}{R_{Li}} & \frac{1}{R_{Lo}} & & & -\frac{1}{R_{Lr}} - \frac{1}{R_{Li}} - \frac{1}{R_{Lo}} \end{bmatrix}$$

References

1. Li, Q.H., Hamilton, J.F.: Investigation of the transient response of a dual-rotor system with intershaft squeeze-film damper. J. Eng. Gas Turb. Power **108**, 613–618 (1985)
2. Holmes, R., Dede, M.M.: Non-linear phenomena in aero-engine rotor vibration. Arch. Proc. Inst. Mech. Eng. Part A J. Power Eng. **203**(11), 25–34 (1989)
3. Yamamoto, T.: On critical speeds of a shaft supported by a ball bearing. Trans. JSME **21**, 182–192 (1955)
4. Fukata, S., Gad, E.H., Kondou, T., Ayabe, T., Tamura, H.: On the radial vibrations of ball bearings (computer simulation). Bull. JSME **28**(239), 899–904 (1985)
5. Mevel, B., Guyader, J.L.: Routes to chaos in ball bearings. J. Sound Vib. **162**(3), 471–487 (1993)
6. Tiwari, M., Gupta, K., Prakash, O.: Effect of radial internal clearance of a ball bearing on the dynamics of a balanced horizontal rotor. J. Sound Vib. **238**(5), 723–756 (2000)
7. Tiwari, M., Gupta, K., Prakash, O.: Dynamic response of an unbalanced rotor supported on ball bearings. J. Sound Vib. **238**(5), 757–779 (2000)
8. Ghafari, S.H., Abdel-Rahman, E.M., Golnaraghi, F., Ismail, F.: Vibrations of balanced fault-free ball bearings. J. Sound Vib. **329**(9), 1332–1347 (2010)
9. Bai, C.Q., Zhang, H.Y., Xu, Q.Y.: Subharmonic resonance of a symmetric ball bearing-rotor system. Int. J. Non-Linear Mech. **50**, 1–10 (2013)
10. Zhang, Z.Y., Chen, Y.S., Cao, Q.J.: Bifurcations and hysteresis of varying compliance vibrations in the primary parametric resonance for a ball bearing. J. Sound Vib. **350**, 171–184 (2015)
11. Zhang, Z.Y., Chen, Y.S., Li, Z.G.: Influencing factors of the dynamic hysteresis in varying compliance vibrations of a ball bearing. Sci. China Technol. Sci. **58**(5), 775–782 (2015)
12. Palmgren, A., Ruley, B.: Ball and Roller Bearing Engineering. SKF Industries, inc., Philadelphia (1945)
13. T.A. Harris, M.N. Kotzalas. Essential Concepts of Bearing Technology. Taylor & Francis, London, 2006, pp. 133–135
14. Winer, W.O., Bair, S., Gecim, B.: Thermal resistance of a tapered roller bearing. Tribol. Trans. **29**(4), 539–547 (1986)
15. DeMul, J.M., Vree, J.M., Maas, D.A.: Equilibrium and associated load distribution in ball and roller bearings loaded in five degrees of freedom while neglecting friction—art I: general theory and application to ball bearings. J. Tribol. (1989). https://doi.org/10.1115/1.3261864
16. DeMul, J.M., Vree, J.M., Maas, D.A.: Equilibrium and associated load distribution in ball and roller bearings loaded in five degrees of freedom while neglecting friction—part II: application to roller bearings and experimental verification. J. Tribol. (1989). https://doi.org/10.1115/1.3261865
17. Jorgensen, B.R., Shin, Y.C.: Dynamics of machine tool spindle/bearing systems under thermal growth. J. Tribol. **119**(4), 875–882 (1997)
18. Stein, J.L., Tu, J.F.: A state-space model for monitoring thermally induced preload in anti-friction spindle bearings of high-speed machine tools. J. Dyn. Syst. Meas. Contr. **116**(3), 372–386 (1994)
19. Sun, G., Palazzolo, A., Provenza, A., Lawrence, C., Carney, K.: Long duration blade loss simulations including thermal growths for dual-rotor gas turbine engine. J. Sound Vib. **316**, 147–163 (2008)

20. Takabi, J., Khonsari, M.M.: Experimental testing and thermal analysis of ball bearings. Tribol. Int. **60**, 93–103 (2013)
21. Ai, S.Y., Wang, W., Wang, Y., Zhao, Z.: Temperature rise of double-row tapered roller bearings analyzed with the thermal network method. Tribol. Int. **87**, 11–22 (2015)
22. Than, V.T., Huang, J.H.: Nonlinear thermal effects on high-speed spindle bearings subjected to preload. Tribol. Int. **96**, 361–372 (2016)
23. Wang, N.F., Liu, C., Jiang, D.X., Behdinan, K.: Casing vibration response prediction of dual-rotor-blade-casing system with blade-casing rubbing. Mech. Syst. Signal Pr. **118**, 61–77 (2019)
24. Lu, Z.Y., Chen, Y.S., Li, H.L., Hou, L.: Reversible model-simplifying method for aero-engine rotor systems. J. Aerosp. Power **31**(1), 57–64 (2016)
25. Sun, C.Z., Chen, Y.S., Hou, L.: Steady-state response characteristics of a dual-rotor system induced by rub-impact. Nonlinear Dyn. **86**(1), 91–105 (2016)
26. Gao, P., Hou, L., Yang, R., Chen, Y.S.: Local defect modelling and nonlinear dynamic analysis for the inter-shaft bearing in a dual-rotor system. Appl. Math. Model. **68**, 29–47 (2019)
27. Gao, P., Hou, L., Chen, Y.S.: Nonlinear vibration characteristics of a dual-rotor system with inter-shaft bearing. J. Vib. Shock **38**(15), 1–10 (2019)
28. Yang, R., Jin, Y.L., Hou, L., Chen, Y.S.: Study for ball bearing outer race characteristic defect frequency based on nonlinear dynamics analysis. Nonlinear Dyn. **90**, 781–796 (2017)
29. Hou, L., Chen, Y.S., Fu, Y.Q., Chen, H.Z., Lu, Z.Y., Liu, Z.S.: Application of the HB-AFT method to the primary resonance analysis of a dual-rotor system. Nonlinear Dyn. **88**(4), 2531–2551 (2017)
30. Holman, J.P.: Heat Transfer, 10th edn, pp. 51–52. McGraw Hill, New York (2010)
31. Muzychka, Y.S., Yovanovich, M.M.: Thermal resistance models for non-circular moving heat sources on a half space. J. Heat Transf. **123**(4), 624–632 (2001)
32. Fand, R.M.: Heat transfer by forced convection from a cylinder to water in crossflow. J. Heat Mass. Transf. **8**(7), 995–1010 (1965)
33. Gazley, C.: Heat-transfer characteristics of the rotational and axial flow between concentric cylinders. Trans. ASME **108**, 79–90 (1958)
34. Yang, Z.L., Zhuo, X.R., Yang, C., Song, Y.Z.: An experimental research on convective heat transfer on the surface of horizontal cylinder rotating with high speed. Ind. Heat. **5**, 17–20 (2002)
35. Ruhe, A.: Properties of a matrix with a very ill-conditioned eigenproblem. Numer. Math. **15**(1), 57–60 (1970)
36. Hu, Q.H., Deng, S.E., Teng, H.F.: Optimization of rotor-bearing system with nonlinear dynamics considering internal clearance. J. Aerosp. Power **26**(9), 2154–2160 (2011)